RSC Advances

ROYAL SOCIETY OF CHEMISTRY

www.rsc.org/advances

Synthesis, Growth and Photoluminescence Behaviour of $Gd_2O_2SO_4:Eu^{3+}$ Nanophosphors: The Effect of Temperature on the Structural, Morphological and Optical Properties

R. Manigandan,[a] K. Giribabu,[a] R. Suresh,[a] S. Munusamy,[a] S. Praveen kumar,[a] S. Muthamizh,[a]

T. Dhanasekaran, A. Padmanaban,[a] and V. Narayanan*[a]

[a]*Department of Inorganic Chemistry, University of Madras, Guindy Campus, Chennai 600025.*

* E-mail: vnnara@yahoo.co.in

Fax: +91-44-22300488; Tel: +91-44-22202793

Abstract.

$Gd_2(SO_4)_3 \cdot 8H_2O$, $Gd_2O_2SO_4$, and $Gd_2O_2SO_4:Eu^{3+}$ nanoparticles have been synthesized in the presence of Gd^{3+} ion and sodium dodecyl sulphate (SDS) by the simple complexation-thermal decomposition (CTD) method. The structural analysis, growth mechanism and optical properties of the $Gd_2(SO_4)_3 \cdot 8H_2O$, and $Gd_2O_2SO_4$ is described by diffraction pattern, functional group analysis, Raman, morphology, elemental analysis, and absorbance spectra. The most intriguing future was that the $Gd_2O_2SO_4$ nanoplates are in the range of 42-50 nm without adding any external stabilizer. The study results revealed that the $Gd_2O_2SO_4$ nanoparticles with orthorhombic structure are having a band gap of 3.12 eV. Furthermore, $Gd_2O_2SO_4$ shows an intense red photoluminescence associated with the $^5D_0 \rightarrow {}^7F_2$ transition in the presence of Eu^{3+}. The results suggest that the $Gd_2O_2SO_4:Eu^{3+}$ nanophosphors, may have a beneficial approach in the field of biomedical application as luminescent probe/labels.

Key words: Gadolinium oxysulfate, gadolinium dodecyl sulphate, growth mechanism, hierarchical nanostructure, band gap, photoluminescence.

1. Introduction.

Phosphors have stimulated intensive interest within the researchers in the last few years, due to their technological importance and scientific application. Rare earth (RE) phosphors with unique physic-chemical properties (magnetic, electrical, electronic, optical and so forth) makes them critically important in magnets, superconducting and electronic material, medical imaging and cancer therapy, pigments, phosphor screens and fluorescent materials.[1-6] It is important the systematic research of the rare earth hosted in different kind of crystals with good structural, morphology, and optical properties as an efficient emitting material. The optical activation of RE ions doped crystals can be enhanced significantly because of energy transfer from host and charge transfer to RE[7]. Especially, Eu^{3+} ion ($4f^6$) results very intense luminescence in the red region (610-620 and 690-710 nm). The red emission is included to the biological window, which can be used in many display applications. These red emitter nanoparticles (RENPs) are used in biomedical applications as luminescence probes/labels. In particular, the nanostructured rare-earth compounds with high unpaired f-electron spin values have been applied to the biomedical field of therapeutic agent, MRI contrast agent, single phase multifunctional bio-probes and drug delivery host matrix for upconversion fluorescence.[8-11]

Rare earth oxysulfate ($RE_2O_2SO_4$) has considered as a host matrix for activates the electronic transition with the Eu^{3+} ions to reveals luminescence. Not only $RE_2O_2SO_4$, but also several fluorides, [12] molybdates, [13] phosphates, [14] and sulfites [15] have also been reported as the host crystals of phosphor. Amongst, $RE_2O_2SO_4$ has some unique chemical and optical features, such as low toxicity, sharp emission lines, high magnetic moment due to the seven unpaired electrons ($^8S_{7/2}$), and long lifetimes.[16, 17] It was well known that, the behaviour of nanostructured materials

purely depends on their particle size and shape.[18] In addition, it has been widely reported that the bulk to nanoscale size reduction play the major role on the physiochemical properties of various nanomaterials.[19] synthesis of advanced materials with controlled size and/or polydispersity to obtain improved or novel properties by using colloidal assemblies as templates[20]. Anionic surfactant like sodium dodecyl sulphate (SDS) was good candidate for controlling the size and shape of nanoparticles in various methods including thermal and nonthermal method.[21, 22] Gadolinium, the most abundant element in the rare-earth metal family has notable importance, because of its high magnetic moment due to the seven unpaired electrons ($8S_{7/2}$). However, relatively few publications about the synthesis, controlled size and growth mechanism of $Gd_2O_2SO_4$ have been reported and the resulting products are limited to needle-like hierarchical and plate morphology. The focus of this work has been to explore the structural, growth, and optical property of size-reduced $Gd_2O_2SO_4$ obtained by absence of any external capping agents. Interestingly, dodecyl sulphate itself acts as a complexing agent as well as size controller. To the best of our knowledge, the investigation on growth mechanism of gadolinium oxysulfate from gadolinium dodecyl sulphate by the simple complexation-thermal decomposition (CTD) method has not been reported so far. In this present work, $Gd_2(SO_4)_3 \cdot 8H_2O$, $Gd_2O_2SO_4$ nanoparticles and $Gd_2O_2SO_4$:Eu^{3+} nanophosphors were synthesized by the simple CTD method. The synthetic experiments indicate that the formation of gadolinium dodecyl sulphate needle-like hierarchical nanostructure is through the reaction between Gd^{3+} and DS^- ions by an orientation mechanism. The oriented nanoneedles deformed to plate-like nanostructure by the Ostwald ripening method. Growth mechanism, crystal structure, optical band gap, morphology, and photoluminescence property of $Gd_2O_2SO_4$ have been investigated.

2. Experimental section

2.1. **Materials.**

Gadolinium(III) nitrate hexahydrate ($Gd(NO_3)_3 \bullet 6H_2O$, 99.9%), and europium(III) acetate hydrate ($Eu(CH_3CO_2)_3 \bullet H_2O$, 99.9%) was purchased from Sigma-Aldrich. Sodium dodecyl sulphate ($C_{12}H_{25}NaO_4S$, 99%) and ethanol were purchased from SRL India Ltd., and used as received. Double distilled water used as solvent throughout the experiment.

2.2. **Synthesis of the Gadolinium Dodecyl Sulphate (GdDS), Gadolinium Sulphate and Gadolinium Oxysulfate (GdOS).**

Gadolinium dodecyl sulphate was synthesized by reacting stoichiometric amount of gadolinium nitrate and SDS. 0.45 g of gadolinium nitrate was dissolved in 150 mL distilled water and stirred for 20 min. After 20 min, 0.83 g of SDS in 50 mL distilled water was added slowly into the gadolinium nitrate solution. After few seconds the colourless-cloudy colloidal particles were formed. The resulting colourless foam-like product was filtered and washed with de-ionized water. The obtained gadolinium dodecyl sulphate was redispersed in ethanol and evaporated. Further, gadolinium sulphate ($Gd_2(SO_4)_3$), and gadolinium oxysulfate ($Gd_2O_2SO_4$) were obtained by decomposing the gadolinium dodecyl sulphate complex in air atmosphere at 400 °C and 900 °C for 2 h, respectively. The obtained samples were collected for further characterization.

2.3. **Synthesis of the Europium-Doped Gadolinium Oxysulfate (EuGdOS).**

5% (w/w) Europium-doped gadolinium oxysulfate $(Gd_{0.95}Eu_{0.05})_2O_2SO_4$ was synthesized by the above mentioned CTD method. 0.43 g of gadolinium nitrate and 0.02 g of europium

acetate was dissolved in 150 mL distilled water, which was homogenized for 20 min with stirring. After 20 min, 0.83 g of SDS in 50 mL distilled water was added slowly into the europium-gadolinium nitrate solution. The obtained gadolinium oxysulfate (EuGdOS) by the above mentioned procedure was collected for further analysis.

2.4. **Characterization techniques**

Crystal structure, crystallite size and lattice parameter of the products were determined by Rich Siefert 3000 diffractometer with Cu $K_{\alpha 1}$ radiation (λ = 1.5406 Å). Fourier Transform Infrared Spectroscopy (FTIR) spectra were recorded on a Perkin Elmer FTIR spectrophotometer in the region of 4000 to 400 cm^{-1}. The morphology was analyzed by HITACHI SU6600 (FE-SEM) Field Emission Scanning Electron Microscopy coupled with Energy Dispersive X-ray analysis (EDAX) and High Resolution Transmission Electron Microscopy (HRTEM) using a FEI TECNAI G^2 model T-30 at accelerating voltage of 250 kV. Raman spectrum was recorded using laser confocal microscope, Raman-11 Nanophoton Corporation, Japan and Ultraviolet-Visible Diffuse Reflectance spectroscopy (DRS-UV-Vis) was recorded using Perkin Elmer lambda650 spectrophotometer. Photoluminescence spectra were recorded using a Perkin-Elmer LS5B luminescence spectrophotometer.

3. Results and discussion

Gadolinium oxysulfate nanoparticles were synthesized by a simple approach involving calcination of gadolinium dodecyl sulphate complex. The dodecyl sulphate (DS^-) self-assembled with gadolinium nitrate by complexation method was re-dissolved in ethanol to form a transparent colloidal solution under ambient condition. GdDS complex results numerous products including gadolinium sulphate and gadolinium oxysulfate at various condition. The

graphical representation of possible growth mechanism was shown in scheme 1. The X-ray diffraction (XRD) pattern of the prepared sample calcined at (a) 400 °C, (b) 700 °C, and (c) 900 °C were given in Figure 1. The powder XRD pattern in Figure 1a, all the diffraction peaks could be indexed to the end centered monoclinic phase matched with standard value (JCPDS. No: 081-1794) of $Gd_2(SO_4)_3 \cdot 8H_2O$, with C2/c (15) space group. The lattice constants were calculated using the XRD pattern, a=11.97 Å, b=7.09 Å, c=17.95 Å. In Figure 1b, the mixed phase of (a) and (c) occur in the calcination at 700 °C, which gives clue about the phase transformation from $Gd_2(SO_4)_3$ to GdO_2SO_4, which has grown on (013) plane. When the temperature was raised to 900 °C, well defined diffraction peaks appeared and the lattice parameters (a=4.04 Å, b=4.17 Å, c=12.97 Å) could be indexed to the orthorhombic phase of $Gd_2O_2SO_4$ matched with the standard value (JCPDS. No: 029-0613) of $Gd_2O_2SO_4$, suggesting that the $Gd_2(SO_4)_3$ crystal structure has been converted into $Gd_2O_2SO_4$. The similarity of peak broadening in the entire diffraction patterns indicates there were no vast changes in crystallite size. The FTIR spectrum showed in Figure 2 depicts the changes occurring in the GdDS under the various heat treatment conditions (100 °C to 900 °C). The obtained peaks were assigned to S-O asymmetric stretching vibration at 1236 cm^{-1}, and symmetric stretching vibration at 1060, and 1004 cm^{-1}. The peaks at 2976, 2914, 2854, and 823 cm^{-1} were assigned as C-H stretching and bending modes.[24] Figure 2 demonstrates characteristic broad intense bands in the range of 3000-3750 cm^{-1}, and 1620 cm^{-1} were corresponds to the H-OH vibrations. The peaks near 1384 and 1523 cm^{-1} were assigned to the impurities like C-O absorbed on the sample surface at the decomposition stages. The peaks in the region of 570 to 670 cm^{-1} corresponds to the vibration of Gd-S bond and 526 cm^{-1} corresponds to the vibration of Gd-O bond.[25] In FTIR spectrum, the deformation of H-OH and C-H and the

appearance of Gd-O bond at corresponding decomposition stages clearly explain the growth mechanism of $Gd_2(SO_4)_3$, and $Gd_2O_2SO_4$ from gadolinium dodecyl sulphate.

Figure 3a, and 3b shows the FESEM-EDAX images of the as prepared GdDS, which clearly indicates that the product consists of cactus needle-like nanorices assembled by orientation mechanism. The high magnification FESEM image (Figure 3b) exhibits the formation of needle shaped particle with sharp headed tips. The inspection of images suggests that the coalescence between the particles may contribute to the growth by the orientation mechanism in the complexation method. In addition, the elemental analysis was obtained by EDAX analysis, shown in Figure 3c, which clearly demonstrates a homogeneous distribution of gadolinium, carbon, oxygen, and sulphur elements. HRTEM images of GdDS shown in Figure 4a and 4b reveals that the observed results well-matched with the FESEM results. In agreement with the FE-SEM results, the average breadth in the middle part of needles was measured in the range of 50-55 nm. Selected area energy diffraction (SAED) pattern shown in Figure 4c reveals that the nanoneedles were highly crystalline in nature. The Figure 5a represents FESEM-EDAX images of hydrated $Gd_2(SO_4)_3$ at 400 °C, reveals that the particles were close to elongated spheroids with aggregation due to the temperature. Ripening at this stage leads to the formation of elongated spheroid shaped particle from melted needles. FESEM-EDAX images of sample at 700 °C shown in Figure 5b reveals that the shape transformation from spheroid into plate shape has taken place. According to the results the possible formation mechanism of the cactus needle like nanorices, the experimental results could be explained as follows. Self-assembly of surfactant (SDS) will results the formation of oil-in-water aggregates, commonly called as micelles. To make particles, the metal ion of the surfactant (sodium) is replaced by the reactive ion (Gadolinium) in the chemical reaction. The increasing concentration of SDS concentration

acts as one of the reactant, which reduces flocculation and stimulates the formation of well-defined particles due to the inherent van der Waals attraction between particle and dispersion forces. [21, 26] While increasing temperature at the thermal decomposition state the ripening process takes place due to the thermal diffusion of ions, which induces the structural and shape deformation. The following inspection of the results reveals that the formation of GdDS nanorices obtained by the orientation mechanism and further growth process begun to nanoplates from nanorices by the Ostwald ripening mechanism. The growth of the plate like structure was further confirmed by the FESEM-EDAX images of sample calcined at 900 °C shown in Figure 5c, which evidences the presence of gadolinium, oxygen, sulphur and absence of carbon elements, and it was in good agreement with the results shown above.

Figure 6 shows the absorption spectra of the GdDS nanoparticles calcined at different temperatures 400, 700, and 900 °C, respectively, carried out using DRS UV–Vis spectrometer, in order to characterize the optical absorbance properties. It can be seen from spectra for samples calcined at 700, and 900 °C temperatures, the UV absorption in the region of short wavelength consist of a significant broad band at 240 nm, small hump at 274 nm and the predominant peak at 344 nm. While increasing the calcination temperature of GdOS nanoparticles from 700 to 900 °C, the relative intensity of the two broad band's increases significantly, this elucidates that the intensity of the composed bands strongly depends on the calcination temperature. The absorption band near short wavelength region at 344 nm in the spectra can be related to the transition from the ground state of $^{8}S_{7/2}$ to emitting state $^{6}P_{7/2}$ of Gd^{3+} ion.[27, 28] The weaker absorption band located at 240 nm was due to the transition from the 2p orbitals of O^{2-} to the 4f orbitals Gd^{3+} ion, the band ascribed to the absorption of $Gd_2O_2SO_4$ host crystal. Another peak with weak

absorption at 274 nm was attributed to the $^8S_{7/2}$ to $^6I_{7/2}$ internal f-f transition.[29] The band gap (Eg) of the $Gd_2O_2SO_4$ can be calculated from Tauc equation.

$$\alpha h\nu = A\,(h\nu - Eg)^{1/n}$$

Where α - absorption coefficient, h - Planck constant, ν - frequency, A - constant, and n = 1/2, 2, 3/2, or 3 for direct allowed transition, indirect allowed transition, direct forbidden or indirect forbidden transitions, respectively. The optical band gap of the GdDS calcined at 900 °C inferred from the Tauc plot was shown in Figure 6. The value of hν extrapolated to α = 0 gives the band gap energy of GdOS is approximately 3.12 eV, which exhibits the nature of semiconductivity. The Raman spectra of GdDS under various heat treatment conditions (100 to 900 °C) are shown in Figure 7, recorded at ambient condition. The bands were located in between the region of 60 to 2400 cm^{-1} was listed in Table 1. The D and G bands in the region of 1330-1555 cm^{-1} have disappeared after 400 °C. The disappearance of D and G bands confirms the removal of hydrocarbon from the GdDS and the formation of $Gd_2(SO_4)_3$ begun at 400 °C. Strong band located in the region of 980-1010 cm^{-1} corresponds to the symmetric stretching vibration of SO_4^{2-} ions. However, little signal intensity was observed for the triply degenerate (ν_{as}-SO_4^{2-}) modes in the region of 1080-1170 cm^{-1} in accordance with the weak Raman transition for asymmetric stretching vibrations.[31] After calcination at 700 °C, appearance of new bands in the low frequency region evidences the formation of $Gd_2O_2SO_4$ from gadolinium sulphate. Raman spectrum obtained for GdDS decomposed at 900 °C was corresponding to the gadolinium oxysulfate, is in good agreement with the results reported.[7] The obtained Raman results have good relationship with the discussed FTIR results. Accordingly, temperature consequences the phase transition and the phase was identified to be orthorhombic $Gd_2O_2SO_4$.

FESEM and HRTEM images of $(Gd_{0.95}Eu_{0.05})_2O_2SO_4$ nanoplates were shown in Figure 8b, 8c, respectively. The HRTEM-EDX spectrum of $Gd_2O_2SO_4:Eu^{3+}$ (Fig 8a) confirms the presence of europium in the $Gd_2O_2SO_4$ host. It confirms that successful doping could be attained through current synthetic approach. The HRTEM higher magnification image was shown in Figure 8d, which elucidate that the particles have nanoscale with plate like morphology. The average breadth of the plates was measured in the range of 42-50 nm and the length was estimated to be 520-560 nm. SAED spectrum shown in Figure 8e explains the crystalline nature of the orthorhombic $(Gd_{(0.95)}Eu_{0.05})_2O_2SO_4$ nanophosphors. Europium-doped gadolinium oxysulfate nanophosphors have been calcined for 2 h at 900 °C in order to study the Eu^{3+} emission spectra evolution in the hosts. Eu^{3+} ($4f^6$) were inside orthorhombic $Gd_2O_2SO_4$ nanoparticles, it tends to capture an oxygen 2p electron to move towards the highly stable $4f^7$ configuration.[31, 32] Therefore a low-energy state was created in the triplet state, which was well suited for energy transfer by trivalent europium f-f transition leading to the emission lines for the ($^5D_0 \rightarrow {}^7F_J$ (J=0 to 4) transitions. The photoluminescence spectrum of the $Gd_2O_2SO_4:Eu^{3+}$ were shown in Figure 9. The broad dominant peaks splits as 614, 618 nm arising from the $^5D_0 \rightarrow {}^7F_2$ transition usually associated with Eu^{3+} cations occupying crystallographic sites,[33] which is exist with the displacement of Gd^{3+} by Eu^{3+} ions. The remaining bands have been assigned as $^5D_0 \rightarrow {}^7F_0$ at 578.9 nm, $^5D_0 \rightarrow {}^7F_1$ the group of peaks at 588, 597 nm, $^5D_0 \rightarrow {}^7F_3$ at 657 nm, and $^5D_0 \rightarrow {}^7F_4$ at 701 nm. The $^5D_0 \rightarrow {}^7F_0$ of Eu^{3+} was a transition between two non-degenerate levels. Some weak bands were appeared around its expected location due to the presents of Eu^{3+} ions at defect sites. The 0-0 (zero phonon) line transitions between $^5D_0 \rightarrow {}^7F_0$ gives information on the environment around the doped Eu^{3+} ion at low-symmetry sites in crystal.[34] Moreover, the presence of oxygen in the $Gd_2O_2SO_4$ particles gave rise to a charge transfer (at 400 nm) which could be used to excite the

4f orbital of Eu^{3+} ions more efficiently and the energy position of the lines from trivalent europium ions is basically independent on the host. Orthorhombic $Gd_2O_2SO_4$ nanoplates synthesized by CTD method have a long-term stability and further lanthanide sensitization indispensible and responsible for the optical properties and life science application.

4. Conclusions

A simple method has been developed to synthesize $Gd_2(SO_4)_3$, and $Gd_2O_2SO_4$ by CTD method. The possible growth mechanism is discussed based on the FE-SEM, HRTEM, XRD, FTIR, DRS-UV-Vis, and Raman results. CTD method has a number of advantages including the simple reaction conditions, environmentally friendly, and high reproducibility. The simple CTD method offers a convenient method to synthesize nanostructured materials. This result suggests that the $Gd_2O_2SO_4$ nanophosphors with tailorable nanostructures were hopeful for life science applications as luminescent probe/labels. These finding are important not only for enabling life science application but also for providing sensor platform as well as optoelectronics due to its band gap and emission properties.

FIGURES

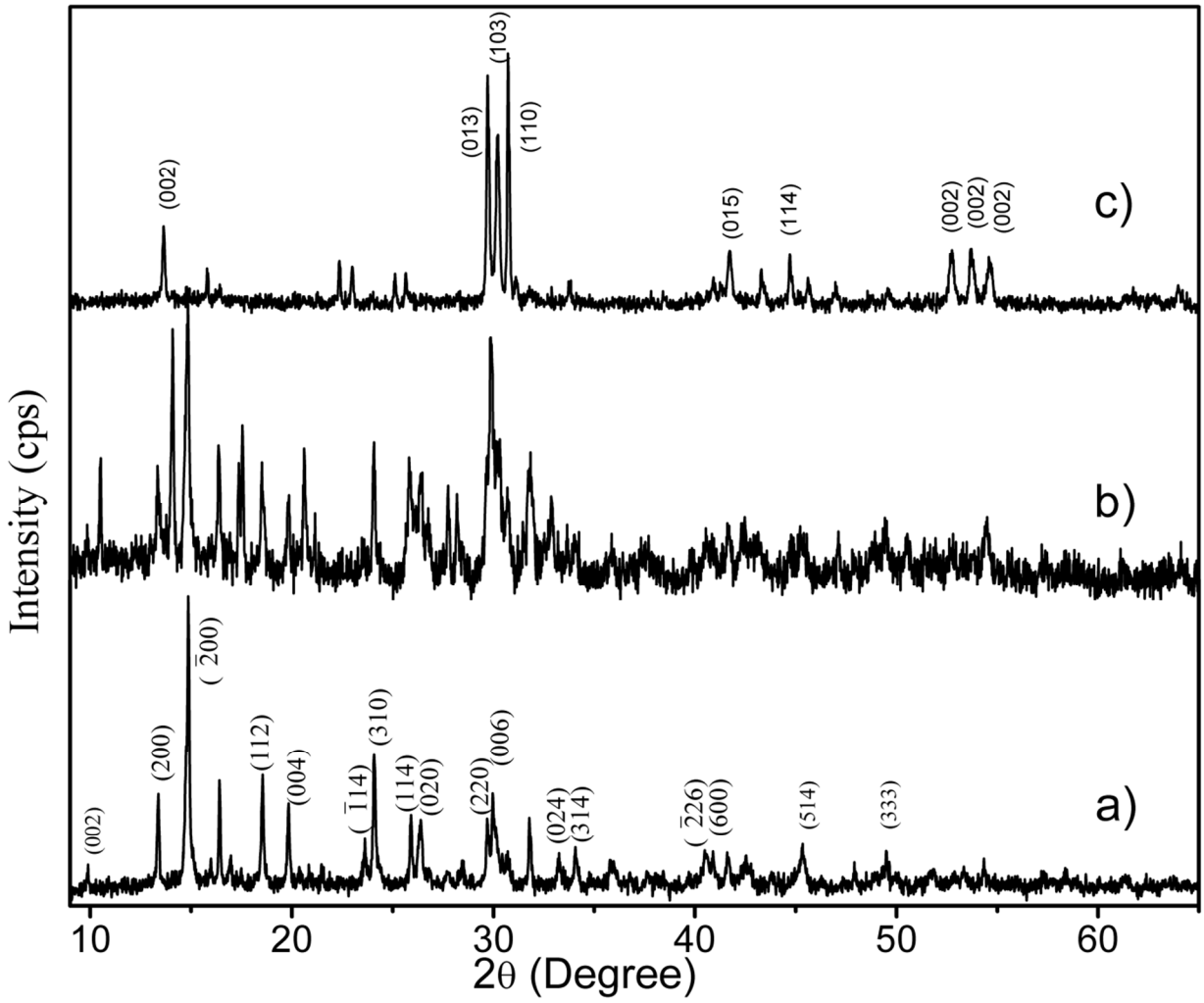

Figure 1. XRD pattern of GdDS decomposed at various temperatures (a) 400, (b) 700, and (c) 900 °C.

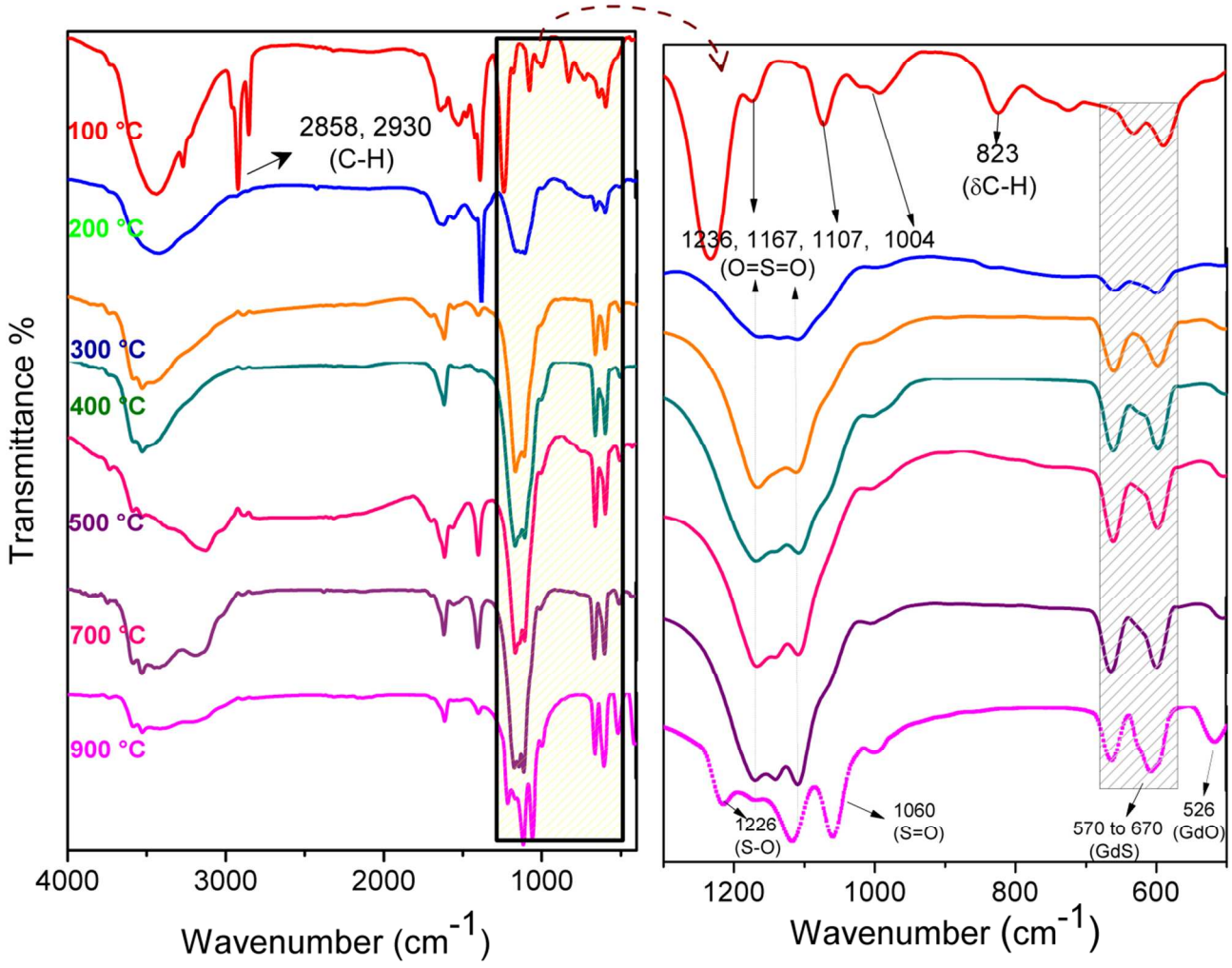

Figure 2. FT-IR spectrum of GdDS decomposed at various temperatures 100, 200, 300, 400, 500, 700, and 900 °C.

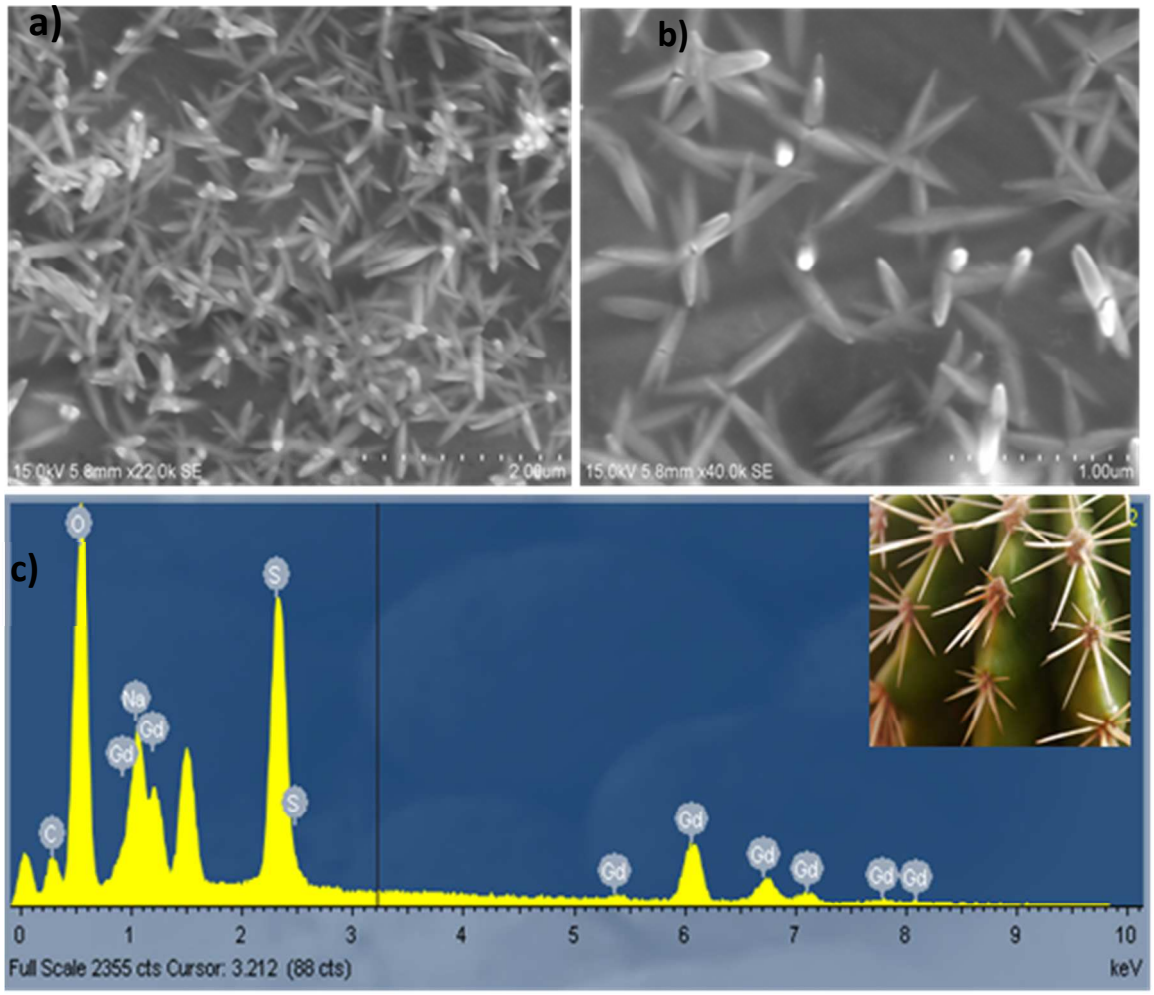

Figure 3. (a). FESEM image of GdDS, (b) high mangnified view of GdDS, and (c) EDAX spectrum of GdDS nanoneedles.

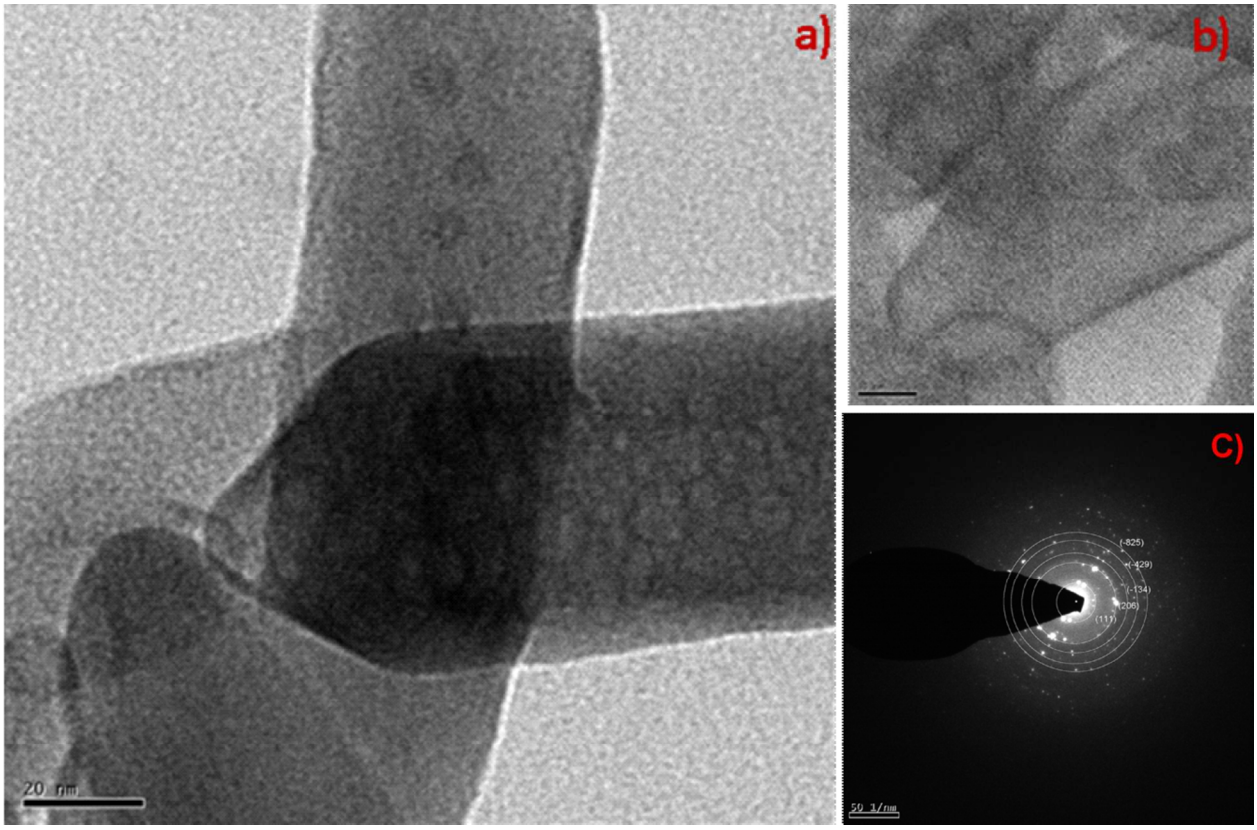

Figure 4. (a). HRTEM image of GdDS, (b) high mangnified view of GdDS, and (c) SAED pattern of GdDS nanoneedles.

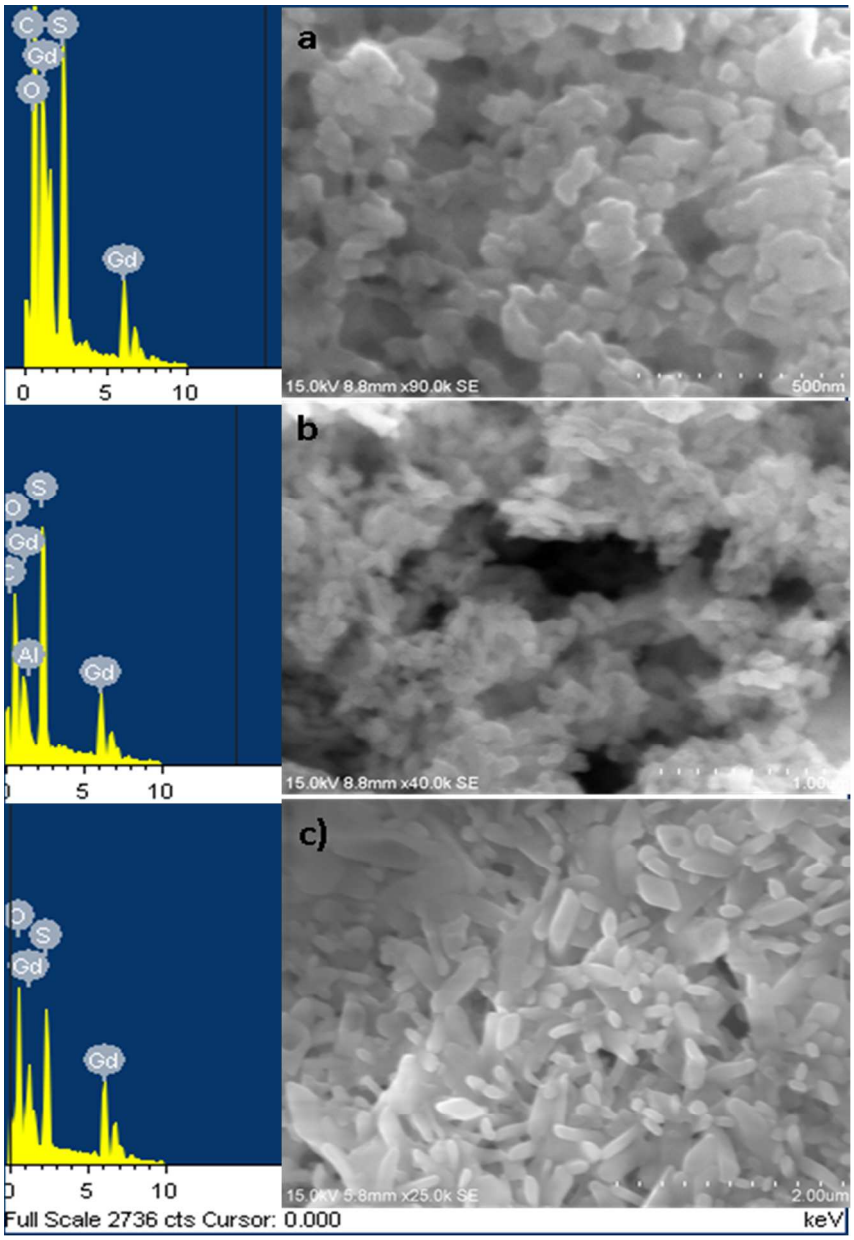

Figure 5. FESEM-EDAX images of GdDS decomposed at various temperatures (a) 400, (b) 700, and (c) 900 °C.

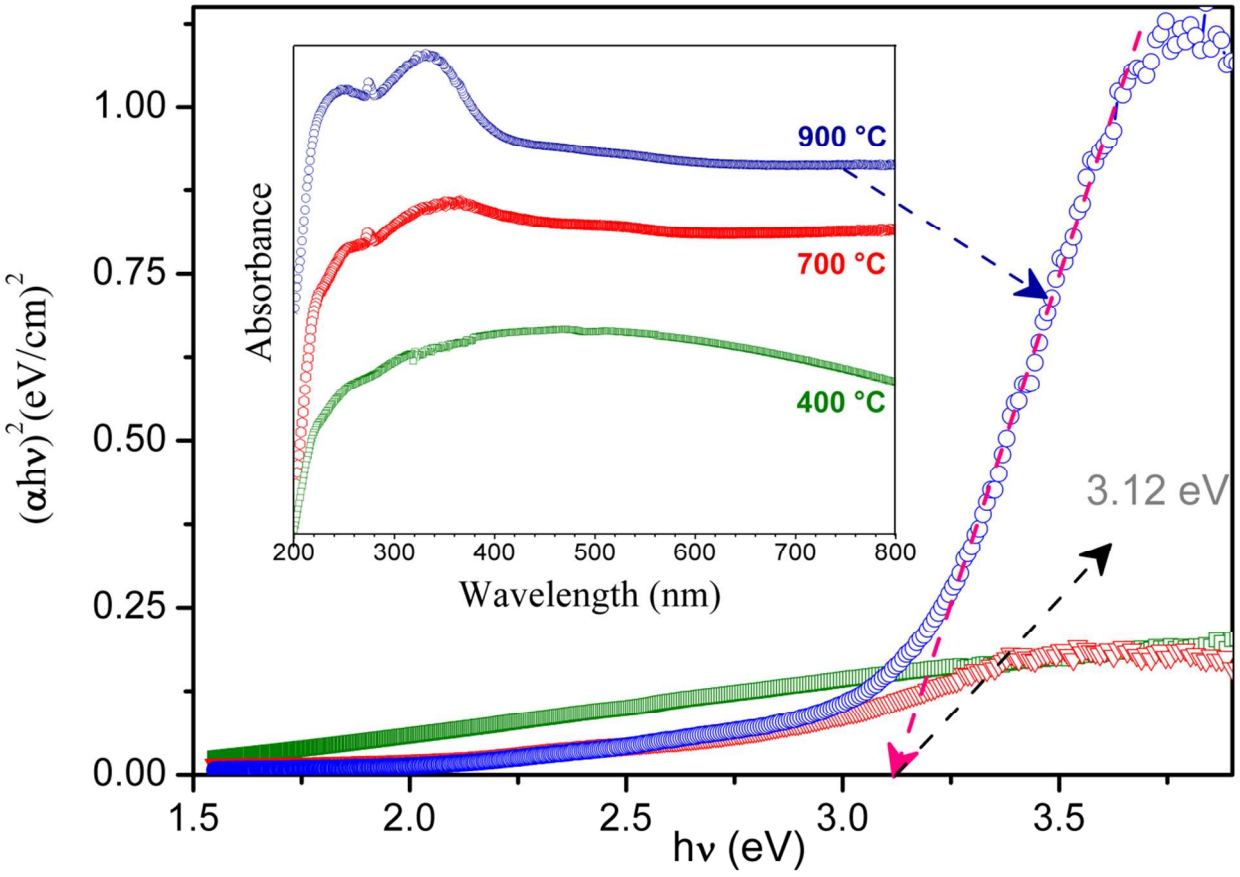

Figure 6. Tauc plot (Inset: DRS-UV-Vis absorption spectrum) of GdDS with optimum conditions.

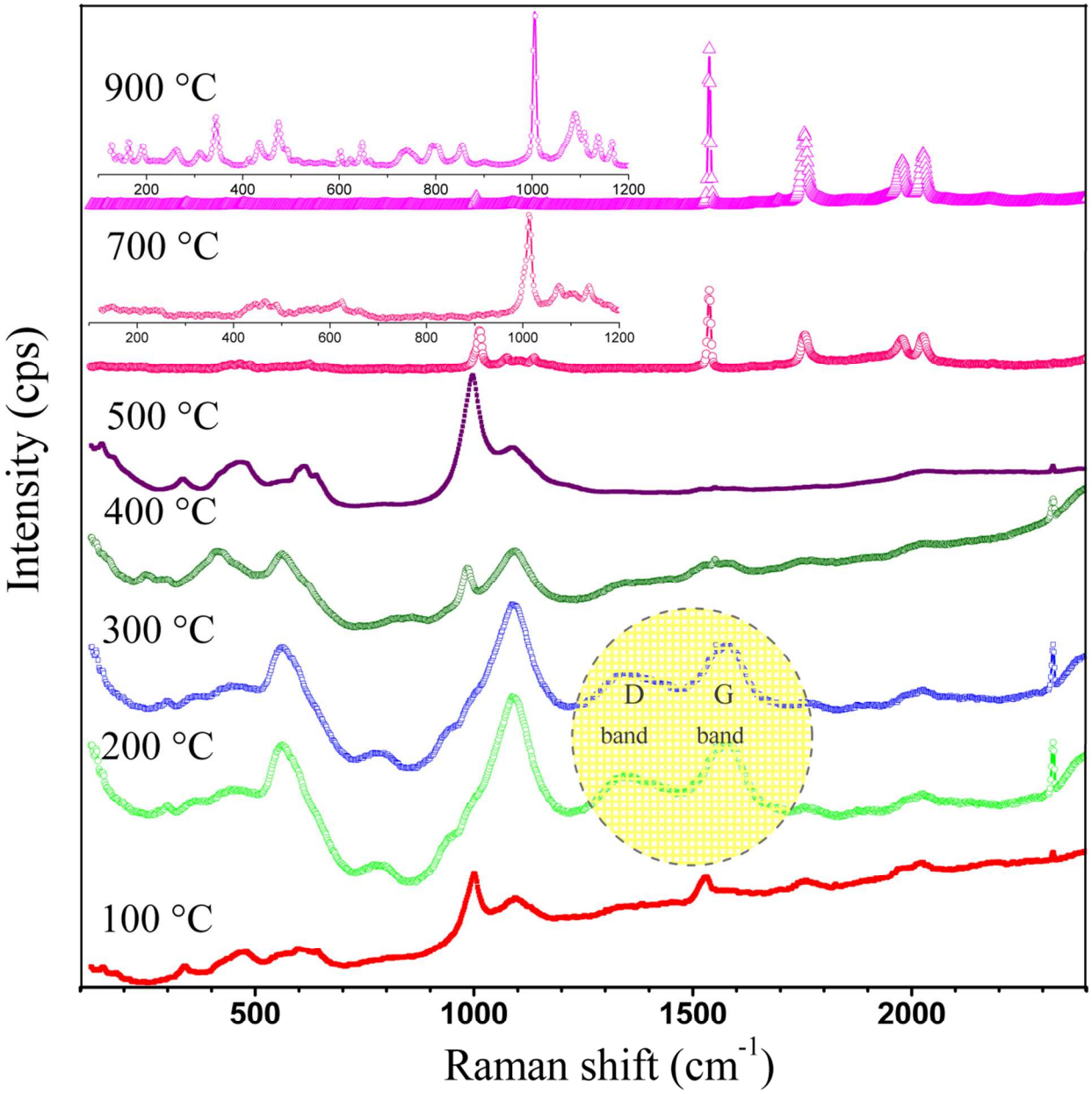

Figure 7. Confocal Raman spectra of GdDS decomposed at various temperatures 100, 200, 300, 400, 500, 700, and 900 °C.

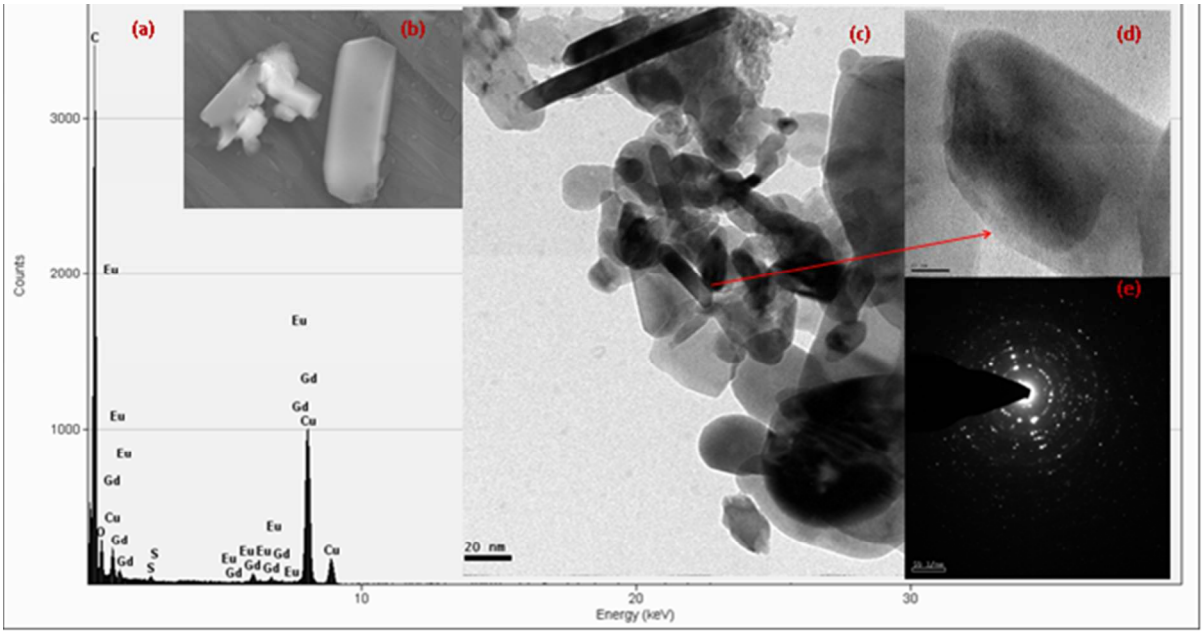

Figure 8. (a) EDX spectrum (b) FESEM image (c) HRTEM image (d) high mangnified view and (e) SAED pattern of $Gd_2O_2SO_4:Eu^{3+}$ nanoplates.

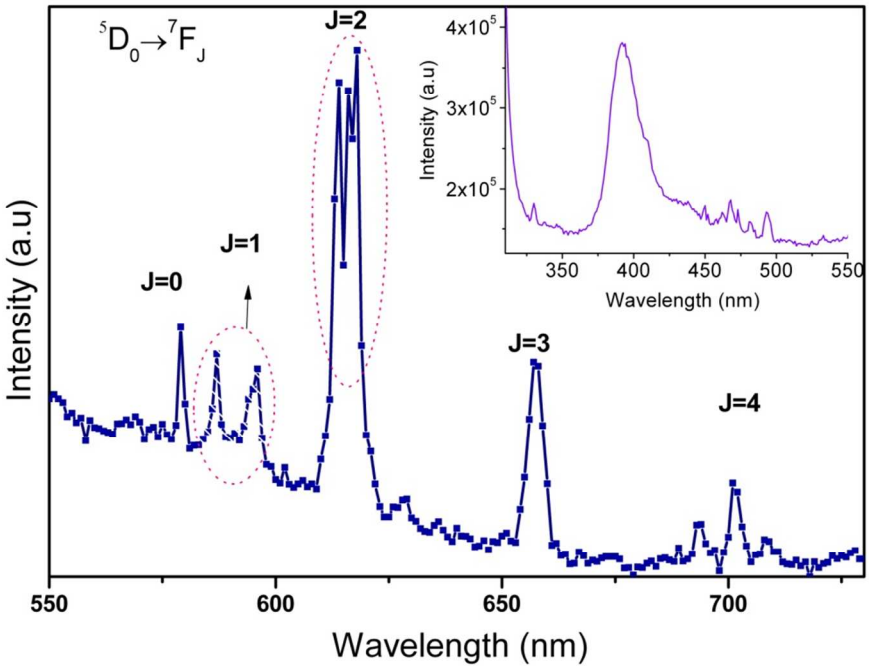

Figure 9. Photoluminescence spectra of $Gd_2O_2SO_4:Eu^{3+}$, Inset: excitation spectrum of $Gd_2O_2SO_4:Eu^{3+}$.

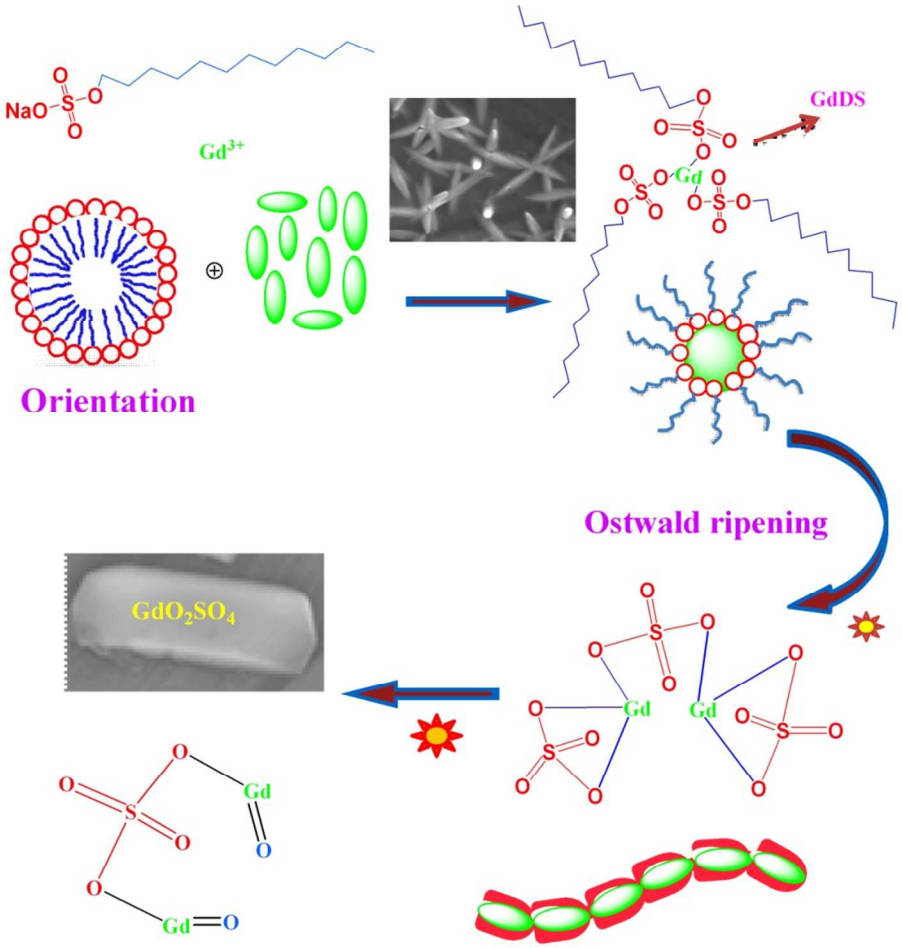

Scheme 1. Schematic representation of the processes occurring at different stages leads to the growth of GdOS nanoplates

Table 1. Raman bands listed for GdDS samples decomposed at various temperatures in the region of 60 to 2400 cm^{-1}

Temperature °C	Raman Bands (cm^{-1})
100	339, 464, 540, 598, 998, 1097, 1357, 1531, 1761, 2030.
200	566, 790, 941, 999, 1082, 1334, 1554, 2026, 2323.
300	423, 564, 790, 1096, 1331, 1551, 2022, 2389.
400	254, 414, 558, 987, 1097, 2325.
500	149, 329, 469, 613, 998, 2330.
700	618, 1002, 1072, 1137, 1557, 1756, 1975, 2030.
900	125, 162,191, 343, 473, 602, 646, 739,794, 852, 1005, 1087, 1135, 1167, 1531, 1697, 1753, 1974, 2030, 2326.

ACKNOWLEDGMENT

The authors acknowledge National Centre for Nanoscience and Nanotechnology, University of Madras for providing financial support and FE-SEM, HRTEM, DRS-UV-Vis and Raman facilities.

REFERENCES

1. K. Bernot, L. Bogani, A. Caneschi, D. Gatteschi and R. Sessoli, *J. Am. Chem. Soc*., 2006, **128**, 7947-7956.
2. S. J. Litzelman, J. L. Hertz, W. Jung, H. L. Tuller, *Fuel Cells,* 2008, **8**, 294-302.
3. L. Faucher, A. A. Guay Begin, J. Lagueux, M. F. Cote, E. Petitclerc and M. A. Fortin, *Contrast Media Mol. Imaging*, 2011, **6**, 209-218.
4. S. Radhika, K. J. Sreeram and B. U. Nair, *ACS Sustainable Chem. Eng.*, 2014, **2**, 1251-1256.
5. Z. Xia and R. Liu, *J. Phys. Chem. C*, 2012, **116**, 15604-15609.
6. J. L. Bridot, D. Dayde, C. Riviere, C. Mandon, C. Billotey, S. Lerondel, R. Sabattier, G. Cartron, A. Le Pape, G. Blondiaux, M. Janier, P. Perriat, S. Roux and O. J. Tillement, *Mater. Chem.*, 2009, **19**, 2328-2335.
7. T. Grzyb, R. J. Wiglusz, V. Nagirnyi, A. Kotlov and S. Lis, *Dalton Trans*., 2014, **43**, 6925-6934.
8. Z. Liu, X. Liu, Q. Yuan, K. Dong, L. Jiang, Z. Li, J. Ren and X. Qu, *J. Mater. Chem.,* 2012, **22**, 14982-14990.
9. G. Tian, Z. Gu, X. Liu, L. Zhou, W. Yin, L. Yan, S. Jin, W. Ren, G. Xing, S. Li and Y. *J.* Zhao, *Phys. Chem. C,* 2011, **115**, 23790-23796.
10. L. Cheng, K. Yang, Y. Li, J. Chen, C. Wang, M. Shao, S. T. Lee and Z. Liu, *Angew. Chem., Int. Ed*., 2011, **50**, 7385-7390.
11. P. Caravan, J. J. Ellison, T. J. McMurry and R. B. Lauffer, *Chem. Rev.,* 1999, **99**, 2293-2352.

12. Q. Zhao, B. Shao, W. Lu, Y. Jia, W. Lv, M. Jiao, and H. You, CrystEngComm, 2013, **15**, 9930-9937.

13. A. K. Parchur, and R. S. Ningthoujam, *Dalton Trans.*, 2011, **40**, 7590-7594.

14. A. I. Prasad, A. K. Parchur, R. R. Juluri, N. Jadhav, B. N. Pandey, R. S. Ningthoujam, and R. K. Vatsa, *Dalton Trans*., 2013, **42**, 4885-4896.

15. F. Wang, X Chen, D. Liu, B. Yang, and Y. Dai, *J. Mol. Struct.,* 2012, **1020**, 153-159.

16. J. Kim, Y. Piao and T. Hyeon, *Chem. Soc. Rev*., 2009, **38**, 372-390.

17. I. F. Li, C. H. Su, H. S. Sheu, H. C. Chiu, Y. W. Lo, W. T. Lin, J. H. Chen and C. S. Yeh, *Adv. Funct. Mater*., 2008, **18**, 766-776.

18. J. Lian, F. Liu, X. Wang and X. Sun, *Powder Technol*., 2014, **253**, 187-192.

19. J. Lian, X. Sun and X. Li, *Mater. Chem. Phys.,* 2011, **125**, 479-484.

20. J. Thirumalai, R. Chandramohan, R. Divakar, E. Mohandas, M. Sekar and P. Parameswaran, *Nanotechnology,* 2008, **19**, 395703(7pp).

21. M. P. Pileni, *Langmuir* 1997, **13**, 3266-3276

22. Y. Lu, X. Tang, L. Yan, K. Li, X. Liu, M. Shang, C. Li and J. Lin, *J. Phys. Chem. C,* 2013, **117**, 21972-21980.

23. M. Machida, K. Kawamura, T. Kawano, D. Zhang and K. Ikeue, *J. Mater. Chem*., 2006, **16**, 3084–3090.

24. J. D. Lee, W. C. Choi and J. D. Kim, *Cryst. Eng. Comm.,* 2010, **12**, 3249–3254

25. R. Manigandan, K. Giribabu, R. Suresh, L. Vijayalakshmi, A. Stephen and V. Narayanan, *Mater. Res. Bull,* 2013, **48**, 4210-4215.

26. J. Liang, R. Ma, F. Geng, Y. Ebina, and T. Sasaki, *Chem. Mater*., 2010, **22**, 6001–6007

27. N. Dhananjaya, H. Nagabhushana, B. M. Nagabhushana, B. Rudraswamy, C. Shivakumara, K. P. Ramesh and R. P. S. Chakradhar, *Physica B: Condensed Matter,* 2011, **406**, 1645-1652.

28. A. Vijayaraj, R. Prabu, R. Suresh, R. Sangeetha Kumari, V. Kaviyarasan, and V. Narayanan, *Bull. Korean Chem. Soc.,* 2012, **33**, 3581-3588.

29. B. Umesh, H. Nagabhushana, S. C. Sharma, B. Eraiah, N. Dhananjaya, B. M. Nagabhushana, J. L. Rao and R. P. S. Chakradhar, *J. Alloys Compd.,* 2014, **591**, 286-292.

30. J. Cejka, J. Sejkora, R. L. Frost and E. C. Keeffe, *J. Raman Spectrosc.,* 2009, **40**, 1464-1468.

31. Y. Song, H. You, Y. Huang, M. Yang, Y. Zheng, L. Zhang and N. Guo, *Inorg. Chem.,* 2010, **49**, 11499-11504.

32. S. A. Osseni, S. Lechevallier, M. Verelst, P. Perriat, J. Dexpert-Ghys, D. Neumeyer, R. Garcia, F. Mayer, K. Djanashvili, J. A. Peters, E. Magdeleine, H. Gros-Dagnac, P. Celsis and R. Mauricot, *Nanoscale,* 2014, **6**, 555-564.

33. A. Escudero, E. Moretti, and M. Ocana, *CrystEngComm*, 2014, **16**, 3274-3283.

34. P. A. Tanner, *Chem. Soc. Rev.,* 2013, **42**, 5090-5101.

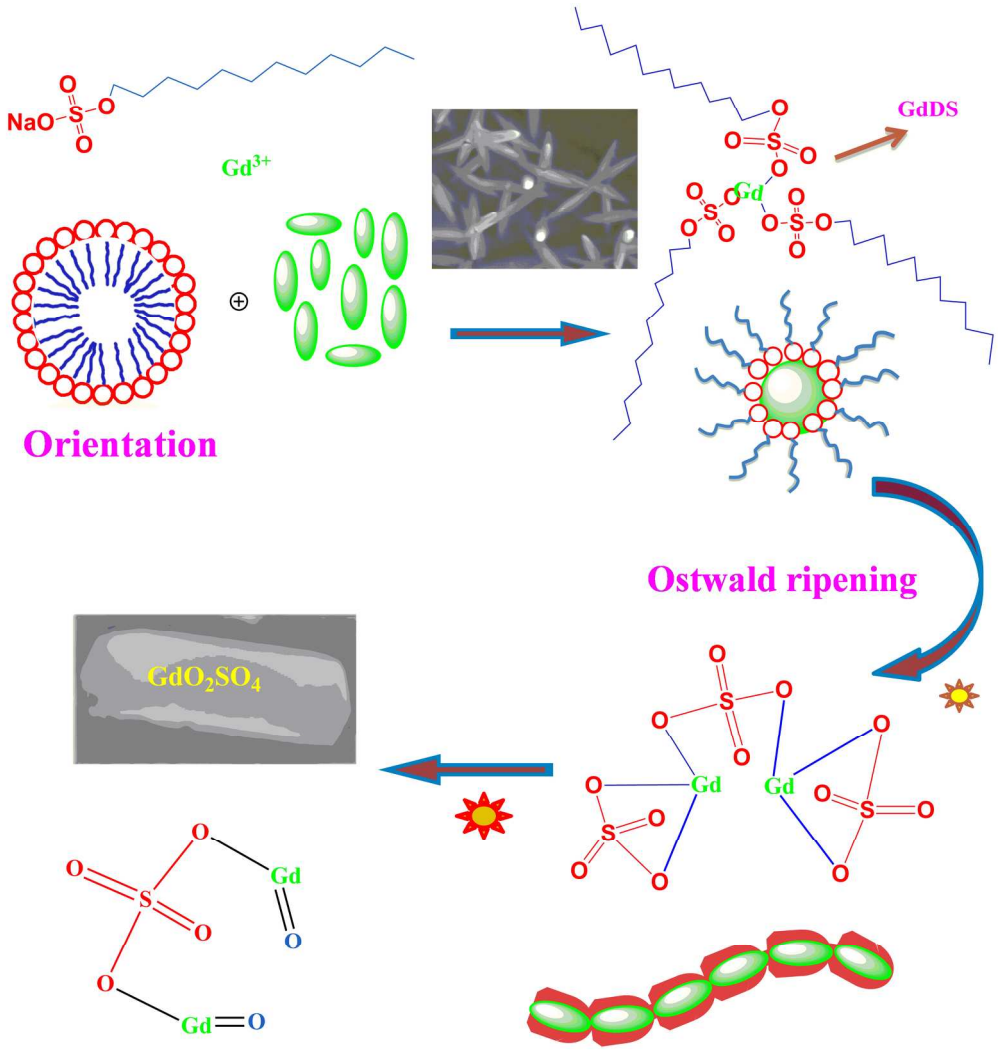

189x198mm (300 x 300 DPI)